Supplement of Atmos. Chem. Phys., 20, 7271–7290, 2020
https://doi.org/10.5194/acp-20-7271-2020-supplement

Atmospheric Chemistry and Physics
Open Access
EGU

Supplement of

The increasing atmospheric burden of the greenhouse gas sulfur hexafluoride (SF_6)

Peter G. Simmonds et al.

Correspondence to: Peter G. Simmonds (petergsimmonds@aol.com)

In this supplementary information we include:

Figure S1. SF_6 model/measurement comparison from the AGAGE 12-box model.

A detailed description of the InTEM and EBRIS inversion models used to estimate regional emissions.

Table S1. InTEM Meteorology.

Table S2. Rand Corporation sales of SF6 to End-Use applications.

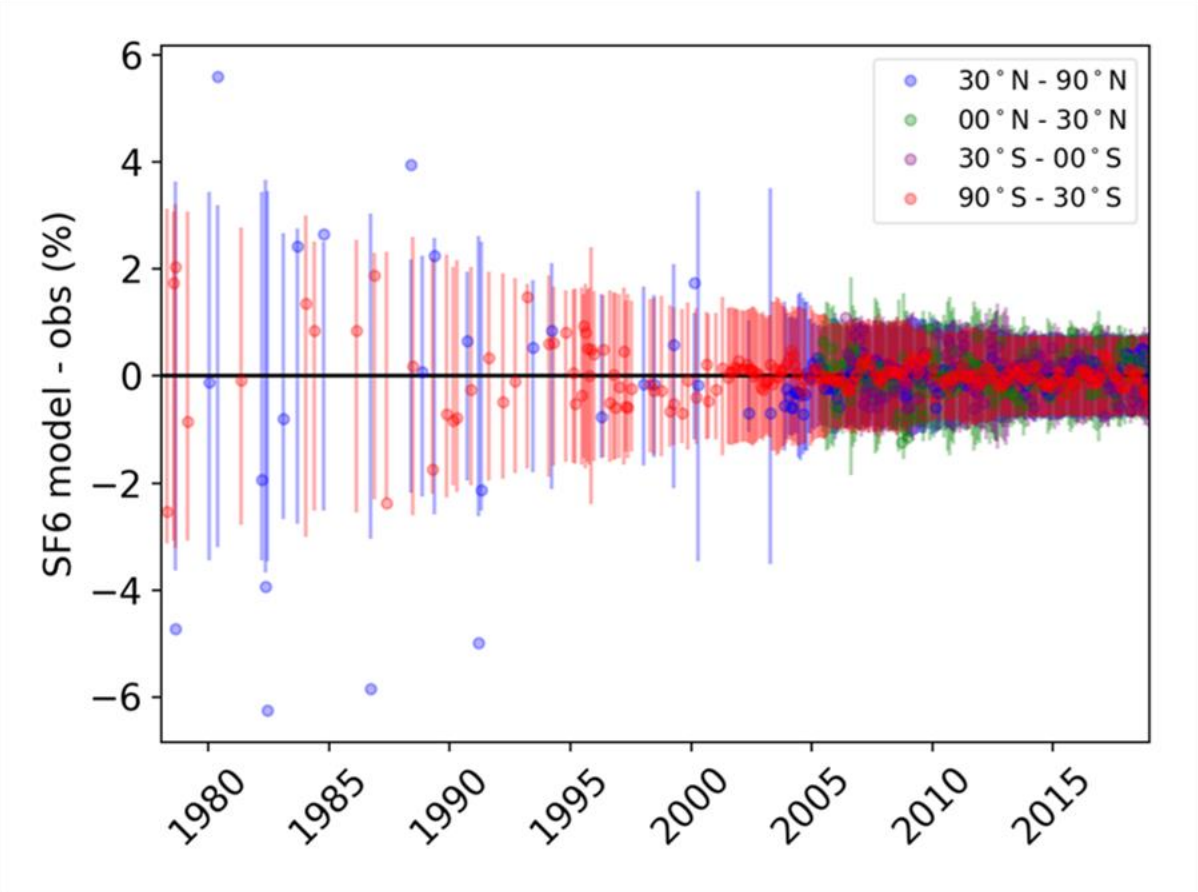

Figure S1. SF_6 model/measurement comparison from the AGAGE 12-box model.

InTEM model description

InTEM is a Bayesian system that minimises the mismatch between the model and the atmospheric observations given the constraints imposed by the observation and model uncertainties and prior information with its associated uncertainties. The horizontal and vertical resolution of the meteorology has improved over the modelled period and is described in Table ST1. The direction (latitude and longitude) and altitude varying background concentration and observation station bias are solved for within the inverse system along with the spatial distribution and magnitude of the emissions. The time-varying prior background concentration for the DECC network stations is derived from the MHD observations when they are very largely sensitive only to Northern Canada (Arnold et al., 2018), JFJ and CMN prior baselines are derived separately for each station using times when the land influence at these high altitude stations is small. The prior bias (that can be positive or negative) for each station is set to zero with an uncertainty of 0.02 ppt. The population-weighted prior has a total domain uncertainty of 200% and has a domain-wide emission of 2 Gg yr^{-1}. The observations from each station are assumed to have an exponentially decreasing 12-hr time correlation coefficient and, between stations, a 200 km spatial correlation coefficient. The observations are averaged into 2-hr periods. The uncertainty of the observations is derived from the reported daily observation precision uncertainty and the variability of the observations within a 6-hr period. The modelling uncertainty for each 2-hr period at each station varies and is defined as the larger of; the median pollution event in that year at that station, or 16.5% of the magnitude of the pollution event. These values have been derived from analysis of the observations of methane at multiple heights at each station across the DECC network. Each inversion (2-month with 7-sites, 2-yr with 3-sites or 3-yr when only MHD is available) is repeated 24 times, each time 10% of the observations per year per station are randomly removed in 5-day intervals and the results and uncertainty averaged. This random removal of observations allows a greater exploration of the uncertainty, given the potential for some of the emission sources to be intermittent within the time-period of the inversion.

TABLE ST1. 3-DIMENSIONAL METEOROLOGY USED TO DRIVE NAME FOR DIFFERENT YEARS. FOR DECC OBSERVATIONS FROM 2012 ONWARDS THE HIGH RESOLUTION UM METEOROLOGY (LAST LINE) CALCULATED OVER THE UK IS USED NESTED INSIDE THE GLOBAL METEOROLOGY DATA.

Year	Horizontal Resolution	Number Vertical Levels	Time Resolution
Aug 2002 – Dec 2005	~60 km	32	
Dec 2005 – Mar 2011	~40km	32	3hr
Mar 2011 – Jul 2014	~25 km	53	3hr
Jul 2014 – Jul 2017	~17 km	53	3hr
Jul 2017 – Dec 2018	~12 km	53	3hr
Jan 2012 – Dec 2018 (MHD and TAC only)	~ 1.5 km	58	1hr

Arnold, T., Manning, A. J., Kim, J., Li, S., Webster, H., Thomson, D., Mühle, J., Weiss, R. F., Park, S., and O'Doherty, S.: Inverse modelling of CF_4 and NF_3 emissions in East Asia, Atmos. Chem. Phys., 18, 13305-13320, 10.5194/acp-18-13305-2018, 2018.

Cullen, M. J. P.: The unified forecast/climate model, Meteorol. Mag., 122, 81–94, 1993.

Jones, A., Thomson, D., Hort, M., and Devenish, B.: The UK Met Office's next-generation atmospheric dispersion model, NAME III, Air Pollution Modeling and Its Applications Xvii, edited by: Borrego, C. and Norman, A. L., 580–589, 2007.

Definite Empa Bayesian Regional Inversion System (EBRIS)

Surface source sensitivities used by the Empa inverse modelling system were derived with the Lagrangian Particle Dispersion Model (LPDM) FLEXPART (Version 9.1, Stohl et al., 2005) driven by analysis/forecasts from the operational runs of the Integrated Forecast Systems (IFS) of the European Centre for Medium-Range Weather Forecasts (ECMWF). The horizontal resolution of the input data was 0.2°x0.2° over the larger Alpine area and 1°x1° elsewhere. For each observation site 3-hourly release intervals using 50'000 model particles each were defined. These particles were traced backward in time for 10 days. Residence times of the model particles within a regular geographic grid covering Europe and North America and below a sampling height of 100 m were evaluated to derive the source sensitivities.

The regional scale inversion method applied by Empa was described in detail by Henne et al. (2016), where it was applied to CH_4 emissions in Switzerland. The system was applied to various halocarbon emission estimations in Europe (Brunner et al., 2017; Schoenenberger et al., 2018) and East Asia (Vollmer et al., 2018; Lunt et al., 2018; Rigby et al., 2019). The method follows a Bayesian approach in that it optimises the spatiotemporal emission distribution so that simulation and observation of atmospheric concentrations best agree under the restriction of a given a priori emission distribution and its uncertainties. The inversion grid contains variable grid resolution following the average simulated source sensitivity with smaller (larger) grid cells at location with larger (smaller) source sensitivities. The total simulated concentration is separated into the regional contribution covered by the transport model and a baseline fraction. Here, the baseline was estimated from the observed time series at each site separately using the method by Ruckstuhl et al. (2012). The resulting baselines were included as part of the state vector using linear interpolation for times between 5-daily baseline nodes.

The inversion was applied to yearly batches of observations solving for mean annual emissions for the period 2007 to 2016. All valid observations form all sites were used in the inverse estimate. We did not apply any additional filtering of the observations by time-of-day, wind speed or direction. We followed the approach by Stohl et al. (2009) to avoid negative a posteriori emissions in individual grid cells. A priori emissions for SF6 were set to 0.46 Gg yr^{-1} for the whole inversion domain, which covered Western and Central Europe. Emissions were spatially disaggregated proportionally to population densities (Center for International Earth Science Information Network, 2016). A-priori emissions were kept the same for all years. The structure and the values of the covariance matrices for the a priori and data-mismatch uncertainties were described by a set of parameters characterising absolute uncertainty levels and spatiotemporal correlations in the uncertainties (Henne et al., 2016). These parameters included the treatment of autocorrelation in the observations with a temporal correlation length

of 0.25 days. A maximum likelihood approach to obtain the uncertainty parameters as used previously (Henne et al., 2016) did not converge for the current set of inversions. Therefore, these parameters were set based on expert judgment and using an iterative approach to determine the data-mismatch uncertainty (Stohl et al., 2009). The uncertainty of the a priori emissions for the entire inversion domain was set to 100 % .The spatial correlation length scale of the a priori was fixed to a value of 200 km. The uncertainty of the baseline was taken from the fit to the observations (36 ppt, 41 ppt, 80 ppt and 128 ppt for the sites MHD, TAC, JFJ and CMN). A common correlation length scale for the baseline of 30 days was assumed.

Brunner, D., T. Arnold, S. Henne, A. Manning, R. L. Thompson, M. Maione, S. O'Doherty, and S. Reimann, 2017: Comparison of four inverse modelling systems applied to the estimation of HFC-125, HFC-134a, and SF_6 emissions over Europe. *Atmos. Chem. Phys.*, **17,** 10651-10674, doi: 10.5194/acp-17-10651-2017.

Center for International Earth Science Information Network, C. C. U.: Gridded Population of the World, Version 4 (GPWv4): Population Density Adjusted to Match 2015 Revision UN WPP Country Totals. [Available online from http://dx.doi.org/10.7927/H4HX19NJ.]

Henne, S., D. Brunner, B. Oney, M. Leuenberger, W. Eugster, I. Bamberger, F. Meinhardt, M. Steinbacher, and L. Emmenegger, 2016: Validation of the Swiss methane emission inventory by atmospheric observations and inverse modelling. *Atmos. Chem. Phys.*, **16,** 3683-3710, doi: 10.5194/acp-16-3683-2016.

Lunt, M. F., S. Park, S. Li, S. Henne, A. J. Manning, A. L. Ganesan, I. J. Simpson, D. R. Blake, Q. Liang, S. O'Doherty, C. M. Harth, J. Muhle, P. K. Salameh, R. F. Weiss, P. B. Krummel, P. J. Fraser, R. G. Prinn, S. Reimann, and M. Rigby, 2018: Continued Emissions of the Ozone-Depleting Substance Carbon Tetrachloride From Eastern Asia. *Geophys. Res. Lett.*, **45,** 11423-11430, doi: 10.1029/2018GL079500.

Rigby, M., S. Park, T. Saito, L. M. Western, A. L. Redington, X. Fang, S. Henne, A. J. Manning, R. G. Prinn, G. S. Dutton, P. J. Fraser, A. L. Ganesan, B. D. Hall, C. M. Harth, J. Kim, K. R. Kim, P. B. Krummel, T. Lee, S. Li, Q. Liang, M. F. Lunt, S. A. Montzka, J. Muhle, S. O'Doherty, M. K. Park, S. Reimann, P. K. Salameh, P. Simmonds, R. L. Tunnicliffe, R. F. Weiss, Y. Yokouchi, and D. Young, 2019: Increase in CFC-11 emissions from eastern China based on atmospheric observations. *Nature*, 569**,** 546-550, doi: 10.1038/s41586-019-1193-4.

Ruckstuhl, A. F., S. Henne, S. Reimann, M. Steinbacher, M. K. Vollmer, S. O'Doherty, B. Buchmann, and C. Hueglin, 2012: Robust extraction of baseline signal of atmospheric trace species using local regression. *Atmos. Meas. Tech.*, **5,** 2613-2624, doi: 10.5194/amt-5-2613-2012.

Schoenenberger, F., S. Henne, M. Hill, M. K. Vollmer, G. Kouvarakis, N. Mihalopoulos, S. O'Doherty, M. Maione, L. Emmenegger, T. Peter, and S. Reimann, 2018: Abundance and sources of atmospheric halocarbons in the Eastern Mediterranean. *Atmos. Chem. Phys.*, **18,** 4069-4092, doi: 10.5194/acp-18-4069-2018.

Stohl, A., C. Forster, A. Frank, P. Seibert, and G. Wotawa, 2005: Technical note: The Lagrangian particle dispersion model FLEXPART version 6.2. *Atmos. Chem. Phys.*, **5,** 2461-2474, doi: 10.5194/acp-5-2461-2005.

Stohl, A., P. Seibert, J. Arduini, S. Eckhardt, P. Fraser, B. R. Greally, C. Lunder, M. Maione, J. Mühle, S. O'Doherty, R. G. Prinn, S. Reimann, T. Saito, N. Schmidbauer, P. G. Simmonds, M. K. Vollmer, R. F. Weiss, and Y. Yokouchi, 2009: An analytical inversion method for

determining regional and global emissions of greenhouse gases: Sensitivity studies and application to halocarbons. *Atmos. Chem. Phys.*, **9,** 1597-1620, doi: 10.5194/acp-9-1597-2009.

Vollmer, M. K., D. Young, C. M. Trudinger, J. Mühle, S. Henne, M. Rigby, S. Park, S. Li, M. Guillevic, B. Mitrevski, C. M. Harth, B. R. Miller, S. Reimann, B. Yao, L. P. Steele, S. A. Wyss, C. R. Lunder, J. Arduini, A. McCulloch, S. Wu, T. S. Rhee, R. H. J. Wang, P. K. Salameh, O. Hermansen, M. Hill, R. L. Langenfelds, D. Ivy, S. O'Doherty, P. B. Krummel, M. Maione, D. M. Etheridge, L. Zhou, P. J. Fraser, R. G. Prinn, R. F. Weiss, and P. G. Simmonds, 2018: Atmospheric histories and emissions of chlorofluorocarbons CFC-13 ($CClF_3$), CFC-114 ($C_2Cl_2F_4$), and CFC-115 (C_2ClF_5). *Atmos. Chem. Phys.*, **18,** 979-1002, doi: 10.5194/acp-18-979-2018.

Table S2. Rand Corporation Sales of SF_6 to End-Use applications.

	Utilities (Gg)	Equipment (Gg)	*Magnesium (Gg)	*Electronics (Gg)	Adiabatic (Gg)	*Other Uses (Gg)	*Combined Prompt Emissions (Gg)
1996	1.136	4.770	0.530	0.303	0.379	0.454	**1.287**
1997	1.000	4.399	0.200	0.333	0.400	0.333	**0.866**
1998	0.771	4.150	0.119	0.356	0.178	0.356	**0.830**
1999	0.659	3.243	0.152	0.456	0.152	0.405	**1.013**
2000	1.101	3.916	0.184	0.612	0.122	0.184	**0.979**
2001	1.158	4.247	0.193	0.515	0.064	0.257	**0.965**
2002	1.495	3.706	0.325	0.650	0.064	0.325	**1.300**
2003	1.545	3.477	0.258	0.837	0.064	0.322	**1.416**

Note: Values extracted from Rand Report. K. Symthe.: Trends in SF_6 Sales and End-Use Applications: 1961-2003. Rand Corporation. 3rd International Conf. on SF_6 and the Environment 1-2 December 2004.

*Assumes worse case that sales=consumption=emission with Magnesium, Electronics and other uses all being prompt releases.